Airfoil-Wake Modification with Gurney Flap at Low Reynolds Number

Muralikrishnan Gopalakrishnan Meena* and Kunihiko Taira†
Florida State University, Tallahassee, Florida 32310
and
Keisuke Asai‡
Tohoku University, Sendai, Miyagi 980-8579, Japan

DOI: 10.2514/1.J056260

The complex wake modifications produced by a Gurney flap on symmetric NACA airfoils at low Reynolds number are investigated. Two-dimensional incompressible flows over NACA 0000 (flat plate), 0006, 0012, and 0018 airfoils at a Reynolds number of $Re = 1.0 \times 10^3$ are analyzed numerically to examine the flow modifications generated by the flaps for achieving lift enhancement. Although high lift can be attained by the Gurney flap on airfoils at high angles of attack, the highly unsteady nature of the aerodynamic forces is also observed. An analysis of the wake structures along with the lift spectra reveals four characteristic wake modes (steady, 2S, P, and 2P), influencing the aerodynamic performance. The effects of the flap over a wide range of angles of attack and flap heights are considered to identify the occurrence of these wake modes, and are encapsulated in a wake-classification diagram. Companion three-dimensional simulations are also performed to examine the influence of three-dimensionality on the wake regimes. The spanwise instabilities that appear for higher angles of attack are found to suppress the emergence of the 2P mode. The use of the wake-classification diagram as a guidance for Gurney-flap selection at different operating conditions to achieve the required aerodynamic performance is discussed.

Nomenclature

a	=	lift slope
C_D	=	coefficient of drag
$\overline{C_D}$	=	time-averaged drag coefficient
C_L	=	coefficient of lift
$\overline{C_L}$	=	time-averaged lift coefficient
$\overline{C_L/C_D}$	=	time-averaged lift-to-drag ratio
c	=	airfoil-chord length
F_x	=	drag on airfoil
F_y	=	lift on airfoil
f_s	=	vortex-shedding frequency
h	=	Gurney-flap height
l^*	=	characteristic frontal length
Re	=	chord-based Reynolds number
Sr	=	Strouhal number
u_∞	=	freestream velocity
α	=	angle of attack
ν	=	kinematic viscosity
ρ	=	fluid density
ω	=	vorticity

Presented as Paper 2017-0543 at the 55th AIAA Aerospace Sciences Meeting, Grapevine, TX, 9–13 January 2017; received 30 April 2017; revision received 20 October 2017; accepted for publication 25 October 2017; published online 28 November 2017.

*Graduate Research Assistant, Department of Mechanical Engineering and Florida Center for Advanced Aero-Propulsion; mg15h@my.fsu.edu. Student Member AIAA (Corresponding Author).

†Associate Professor, Department of Mechanical Engineering and Florida Center for Advanced Aero-Propulsion; ktaira@fsu.edu. Associate Fellow AIAA.

‡Professor, Department of Aerospace Engineering. Associate Fellow AIAA.

I. Introduction

THE field of low-Reynolds-number aerodynamics has received increased attention over the past couple of decades from the engineering and scientific communities for its fundamental importance, as well as its applications in designing small-scale air vehicles [1–3]; understanding biological flights and swimming [4–7]; and, more recently, uncovering Martian aerodynamics [8–12]. For these applications, the basic understanding of lifting-body aerodynamics in the Reynolds-number range of $Re = 10^2$–10^5 becomes important. Extensive research on this topic has been performed to examine the Reynolds-number effect [1,13], high-angle-of-attack wake dynamics [14–18], wing performance [19,20], flow unsteadiness caused by wing maneuver [13,21–26], and influence of external disturbances [22]. The effect of compressibility is also studied on low-Reynolds-number flows, as Martian air vehicles will likely encounter a range of Mach numbers as they operate in the unique Martian atmosphere [8,9,12,27–29].

Despite the prevalence of low-Reynolds-number aerodynamics research on the aforementioned areas, there has been relatively little work performed on modifying the flowfield around bodies to enhance the aerodynamic characteristics of lifting bodies or alter the behavior of their unsteady wakes in the context of flow control. Whereas a number of work have focused on the use of flow control to suppress separation at moderate Reynolds numbers [30–34], a smaller number of studies have investigated the use of flow control at very low Reynolds numbers to alter the dynamics of unsteady wakes [35–38]. In this work, we consider the use of a simple passive flow-control device, namely, the Gurney flap [39], on symmetric airfoils, and examine its influence on modifying the wake dynamics and aerodynamic characteristics. We have selected the use of a Gurney flap as a flow-modification technique due to its simplicity and its demonstrated ability to modify the flow around wings in higher-Reynolds-number applications.

The initial research on Gurney flaps was conducted by Liebeck [39]. The flaps were tested on a Newman airfoil with its aerodynamic forces analyzed over various angles of attack and flap heights. He hypothesized that the formation of two counter-rotating vortices at the downstream side of the Gurney flap to be responsible for the increase in aerodynamic performance of the airfoil. Later, confirmation of Liebeck's hypothesis and extension of the use of Gurney flaps on race cars were also performed [40,41]. Further research on the physics and vortex dynamics involved with the

attachment of the Gurney flap to the trailing edge of airfoils at a high-Reynolds-number range of $Re = 10^4$–10^6 has been performed with emphasis on uncovering the optimal flap height and deployment strategy at different flight conditions [42–44]. Various numerical and experimental studies have been performed in recent years to study the effects of virtual Gurney flaps [45,46], which are deployed using dielectric-barrier-discharge plasma actuators with the added advantage of being an active flow-control technique.

On the low-Reynolds-number-flow side, studies on wakes at a very low Reynolds number of $Re = 1.0 \times 10^3$ have been performed in literature for airfoils without a Gurney flap attached to the trailing edge [47–49]. One of the few available literatures on incompressible flow over airfoils with a Gurney flap at $Re = 1.0 \times 10^3$ was conducted numerically by Mateescu et al. [50]. Symmetric and cambered NACA airfoils with a Gurney flap attached to the trailing edge were analyzed by the authors. A basic knowledge on the flow physics and aerodynamic forces was also reported. Applications of flow control with Gurney flaps deployed at the trailing edge at high-Reynolds-number flows are examined in the aforementioned studies. On the contrary, the availability of such literature is limited for low-Reynolds-number cases. Moreover, the behavior of the far-field wake structure for both low- as well as high-Reynolds-number flows is not well documented.

In the present work, we perform an extensive parametric study to examine the influence of a Gurney flap on the aerodynamic characteristics and two-dimensional wake patterns behind NACA 0000, 0006, 0012, and 0018 airfoils. In the next section, the computational approach and setup for the study are described. This is followed by the discussion of results from two-dimensional direct numerical simulations (DNS) in Sec. III, in which we first classify the four characteristic wake modes observed. A detailed discussion of each wake mode is also provided. We then examine the effects of the Gurney flap on lift, drag, and lift-to-drag ratio for all airfoils. We also provide in Sec. IV a brief analysis on the spanwise effects on the wake modes by performing companion three-dimensional simulations. Concluding remarks are offered at the end of the paper to summarize the findings and to discuss the potential uses of Gurney flaps.

II. Computational Approach

A. Two-Dimensional DNS

We investigate the influence of Gurney flaps on the two-dimensional wake behind four different symmetric airfoils of NACA 0000 (flat plate), 0006, 0012, and 0018 at a chord-based Reynolds number of $Re \equiv u_\infty c/\nu = 1000$. A wide range of values for the Gurney-flap height and angle of attack are considered in this study for the setup shown in Fig. 1a. The flowfield and force data obtained for each case are analyzed in detail to acquire knowledge on the underlying effect of flow control from the use of the Gurney flap on the airfoils for aerodynamic-performance enhancement.

The problem setup for the current work is depicted in Fig. 1a. Throughout this paper, the length, time, and velocity are nondimensionalized by the chord length c, convective timescale c/u_∞, and the freestream velocity u_∞, respectively, unless otherwise noted. Angles of attack α between 0 and 20 deg are considered for all the airfoils, of which the Gurney flap is attached to the trailing edge perpendicular to the chord line. For all cases, Gurney-flap heights of h/c between 0 and 0.15 are considered. The wing is placed in the domain with its quarter chord at the origin with uniform flow prescribed at the inlet.

For the current analysis, the immersed boundary projection method [54,55] is used to simulate the flow. This method is based on a finite volume formulation and incorporates the no-slip boundary condition along the immersed boundary into the projection operation. The scheme is second-order accurate in time and has a spatial accuracy of higher than first order in the L_2 norm. Moreover, a multidomain technique is used to simulate the flow over a body in free space. The scheme has been validated for a number of cases [14,25], and has been found robust and accurate [55]. Five nested levels of multidomains are used with the finest level being $(x/c, y/c) \in [-1, 1] \times [-1, 1]$ and the largest domain being $(x/c, y/c) \in [-16, 16] \times [-16, 16]$ in size. The time step for all cases is limited to a maximum Courant–Friedrichs–Lewy (CFL) number of 0.3.

In the current study, the drag and lift coefficients are defined as

$$C_D \equiv \frac{F_x}{(1/2)\rho u_\infty^2 c} \quad \text{and} \quad C_L \equiv \frac{F_y}{(1/2)\rho u_\infty^2 c} \tag{1}$$

respectively. The shedding frequency f_s of the lift is non-dimensionalized as the Strouhal number:

$$Sr \equiv \frac{f_s l^*}{u_\infty} \tag{2}$$

in which the characteristic frontal length l^* is taken to be

$$l^* = c \sin(\alpha) + h \cos(\alpha) \tag{3}$$

as illustrated in Fig. 1a. A grid-convergence study was performed on the NACA 0012 airfoil without a flap at $\alpha = 10$ deg for grid size ranging from 200×200 to 500×500. A domain with 360×360 grid resolution was found to be sufficient with less than 1% error in $|C_L|_{\max}$ and Strouhal-number values, also capturing the wake structures effectively. Figure 1b shows the comparison of mean C_L values of NACA 0012 airfoil at $Re = 1.0 \times 10^3$ with past studies [47,48,51–53]. The results obtained from the current simulations are in agreement with the data from the literature.

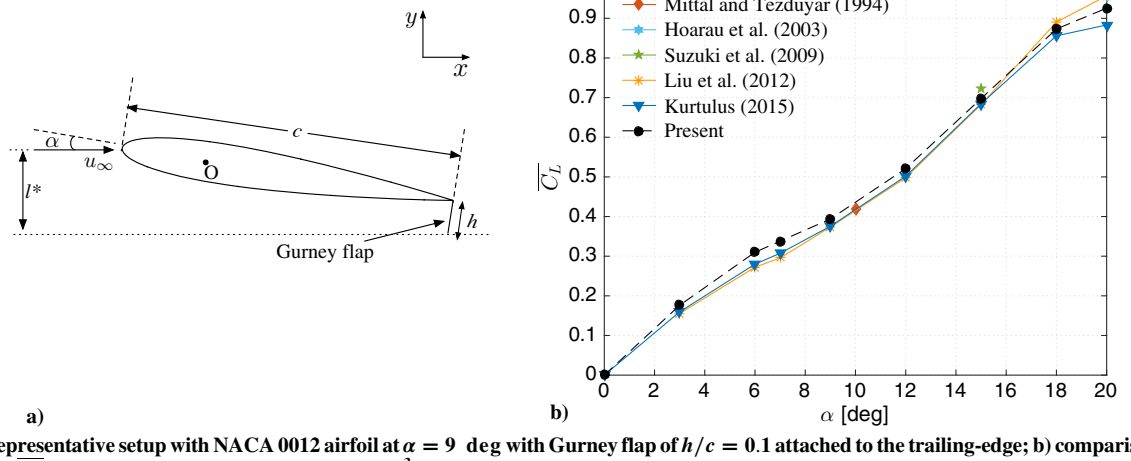

Fig. 1 a) Representative setup with NACA 0012 airfoil at $\alpha = 9$ deg with Gurney flap of $h/c = 0.1$ attached to the trailing-edge; b) comparison of mean lift coefficient $\overline{C_L}$ for NACA 0012 airfoil at $Re = 1.0 \times 10^3$ with previous studies in literature [47,48,51,53].

B. Three-Dimensional DNS

We also perform three-dimensional DNS on selected cases from the two-dimensional analysis to acquire an understanding of the spanwise effects on the wakes. The analysis is performed on the NACA 0006 airfoil with a Gurney flap of $h/c = 0.08$ and $\alpha = 6$, 12, and 18 deg at $Re = 1.0 \times 10^3$. The cases are selected to represent the characteristic wake modes observed from the two-dimensional analysis. We use a finite volume incompressible flow solver, Cliff (CharLES software package), developed by Stanford University and Cascade Technologies to solve the three-dimensional incompressible Navier–Stokes equation [56–59]. A spatial domain of $(x/c, y/c, z/c) \in [-30, 30] \times [-30, 30] \times [0, 4]$ is considered. The spanwise extent of $4c$ is chosen based on a three-dimensional analysis for the baseline cases without a Gurney flap at a similar Reynolds-number range [41,44]. A two-dimensional unstructured spatial grid discretization is used and extruded in the spanwise direction with $\Delta z/c = 0.0625$. The largest nondimensional wall spacings along the suction side of the airfoil are $\Delta x = 0.004$, $\Delta y = 0.007$, and $\Delta z = 0.0625$. The time step for all the simulations is set to a maximum CFL number of 1.0. No-slip boundary condition is specified on the airfoil and Gurney-flap surfaces. An inflow boundary condition of $\boldsymbol{u}/u_\infty = (1, 0, 0)$ is prescribed at the inlet and symmetric boundary conditions at the far-field boundaries (top and bottom). A convective outflow boundary condition is specified at the outflow to allow the wake structures to leave the domain without disturbing the near-field solution. The flow is set to be periodic in the spanwise direction.

A three-dimensional perturbation is introduced to ensure that the three-dimensional structures are sufficiently developed. Temporal convergence of the simulations is ensured through the rms and time-averaged values of pressure and velocities, obtained from a probe data located at the midspan and $1c$ downstream of the trailing edge, having variations less than 2% in time. The solver is validated with previous studies in the literature [48,53] and the current two-dimensional analysis for the NACA 0012 airfoil at $\alpha = 20$ deg with the time-averaged $\overline{C_L}$ having less than 2% difference.

III. Analysis of Two-Dimensional Flows

Findings from the two-dimensional numerical experiments performed for flow over the four NACA airfoils with and without the Gurney flap attached to the trailing edge are discussed here. The addition of the Gurney flap and changes in angle of attack and airfoil thickness bring about various changes to the aerodynamic forces experienced by the airfoils. These variations in the aerodynamic forces are caused by the flow modifications to the airfoil wake. The observations on the airfoil-wake modifications are first discussed, followed by a detailed analysis of the wake dynamics involved through the wake modifications. The effects on the aerodynamic forces are analyzed toward the end of this section.

A. Wake-Mode Classification

First, let us analyze the vorticity field around the airfoils at $Re = 1.0 \times 10^3$ for various Gurney-flap heights and angles of attack. We observe the formation of four distinct types of wakes develop over the airfoil both with and without the Gurney flap.

The numerical simulations reveal that the flowfields can be characterized into four different regimes depending on the characteristics of vortex shedding. The far-field wake developments of different regimes for a representative airfoil setup (NACA 0000 with a Gurney flap of $h/c = 0.06$) are summarized in Fig. 2. The four types of flow regimes observed are 1) steady, 2) 2S (periodic von Kármán vortex shedding), 3) P (periodic shedding of single vortex pairs), and 4) 2P (periodic shedding of two distinct vortex pairs).

These wake modes are classified on the basis of the flow structure of the wake, vortex-shedding frequency, and force fluctuations. In this section, we discuss the difference in the flow structure of the wake modes along with the vortex-shedding frequencies corresponding to each mode. The frequency spectra of the lift history for selected cases of all airfoils are depicted in Fig. 3. Sampling time sufficient to capture 30–50 dominant shedding cycles is used to perform the spectral analysis. The flow transition through the regimes is clearly evident by the abrupt changes in the Strouhal-number values with α for the NACA 0000 case.

The nomenclature of the modes follows the wake-mode classification performed by Williamson and Roshko [60] on the analysis of wakes behind a cylinder in forced oscillation. The wake modes observed in the current study correspond to the 2S, P, and 2P wake modes defined by Williamson and Roshko. These 2S, P, and 2P modes are previously observed in studies involving oscillating cylinder [60–62], as well as airfoils [48,49,63,64]. In particular, the wake modes have also been observed for the baseline case of NACA 0012 airfoil at $Re = 1.0 \times 10^3$ by Kurtulus [48,49].

In the steady regime (Fig. 2, $\alpha = 0$ deg), the wake is steady and the flow is attached to the airfoil surface. This flow regime attributes to the lowest magnitude of drag experienced by the airfoil compared to that in the other unsteady modes. With an increase in α or h/c values, the flow starts to become unsteady. With this, the wake is classified into the next regime, the 2S mode.

The 2S mode (Fig. 2, $\alpha = 6$ deg) is characterized by unsteady flow with periodic von Kármán vortex shedding of alternating clockwise and counterclockwise rotating vortices (2S represents two single vortices). The time-averaged vorticity contour lines are below the center of the wake. The wake height, observable from the time-averaged vorticity fields, is larger compared to that of the steady regime, denoting an increase in drag experienced by the airfoil. The smaller wake height for the 2S regime compared to the other unsteady regimes is also noticed. Also, a single peak in the frequency spectra, corresponding to the vortex-shedding phenomenon, for the cases classified into the 2S regime can be observed in Fig. 3. The Strouhal-number values corresponding to the dominant vortex-shedding frequency lie between [0.12, 0.18] with an increase in angle of attack through this regime. With further increase in α and h/c values, the wake transitions to the next regime, the P mode.

The P mode (Fig. 2, $\alpha = 9$ deg) is distinguished by periodic von Kármán shedding of a single vortex pair (P represents a single vortex pair). The spatial separation between two vortex pairs is distinctly larger compared to that observed between the single vortices in the 2S mode. The time-averaged vorticity contour lines of the regime shift above the center of the wake, portraying a decrease in lift experienced by the airfoil. The height of the wake increases considerably compared to the 2S regime. This increases the drag force experienced by the airfoil. Similar to the 2S regime, the cases classified in the P regime are characterized by the occurrence of single peaks in the frequency spectra, as seen from Fig. 3. The Strouhal number corresponding to these dominant vortex-shedding frequencies saturates to values in $[0.12, 0.18]$ for this regime. Further increase in α and h/c values causes the wake transition to the complex 2P mode.

The 2P mode (Fig. 2, $\alpha = 15$ deg) is characterized by two pairs of vortices convecting above and below the center of the wake (2P represents two vortex pairs). The time-averaged vorticity field for the 2P regime evidently depicts the vortex pairs convecting away from the center of the wake. Compared to all other regimes, the 2P wake is most prominent and has the largest height among the four wake regimes. Consequently, the drag force experienced by the airfoils for this regime is the highest compared to that of all the other modes. Moreover, the downward force acting on the airfoil due to the upward displacement of the mean flow reduces the lift enhancement. The frequency spectra for cases classified in the 2P regime exhibit two prominent peaks, portraying the shedding of the two pairs of vortices. Also, the Strouhal-number values corresponding to the dominant vortex-shedding frequency drop sharply from [0.12, 0.18] and saturate at values $Sr \in [0.06, 0.1]$. These observations from the frequency spectra of the lift compared to that of the 2S and P modes signify the occurrence of the 2P mode. The occurrence of the 2P mode is found in baseline cases (without a Gurney flap) for NACA 0012 at $Re = 1.0 \times 10^3$ by Kurtulus [48,49], but only at very high angles of attack, $\alpha \in [23, 41]$ deg. By adding the Gurney flap, the emergence of the 2P regime is seen for lower α. This 2P mode may be a predominantly two-dimensional phenomenon and may be suppressed by spanwise (three-dimensional) instabilities. We provide discussions on the influence of three-dimensionality on the 2P wake in Sec. IV. Thus, the emergence of the 2P mode should be used as a cautionary guide for the need of three-dimensional simulations to further analyze

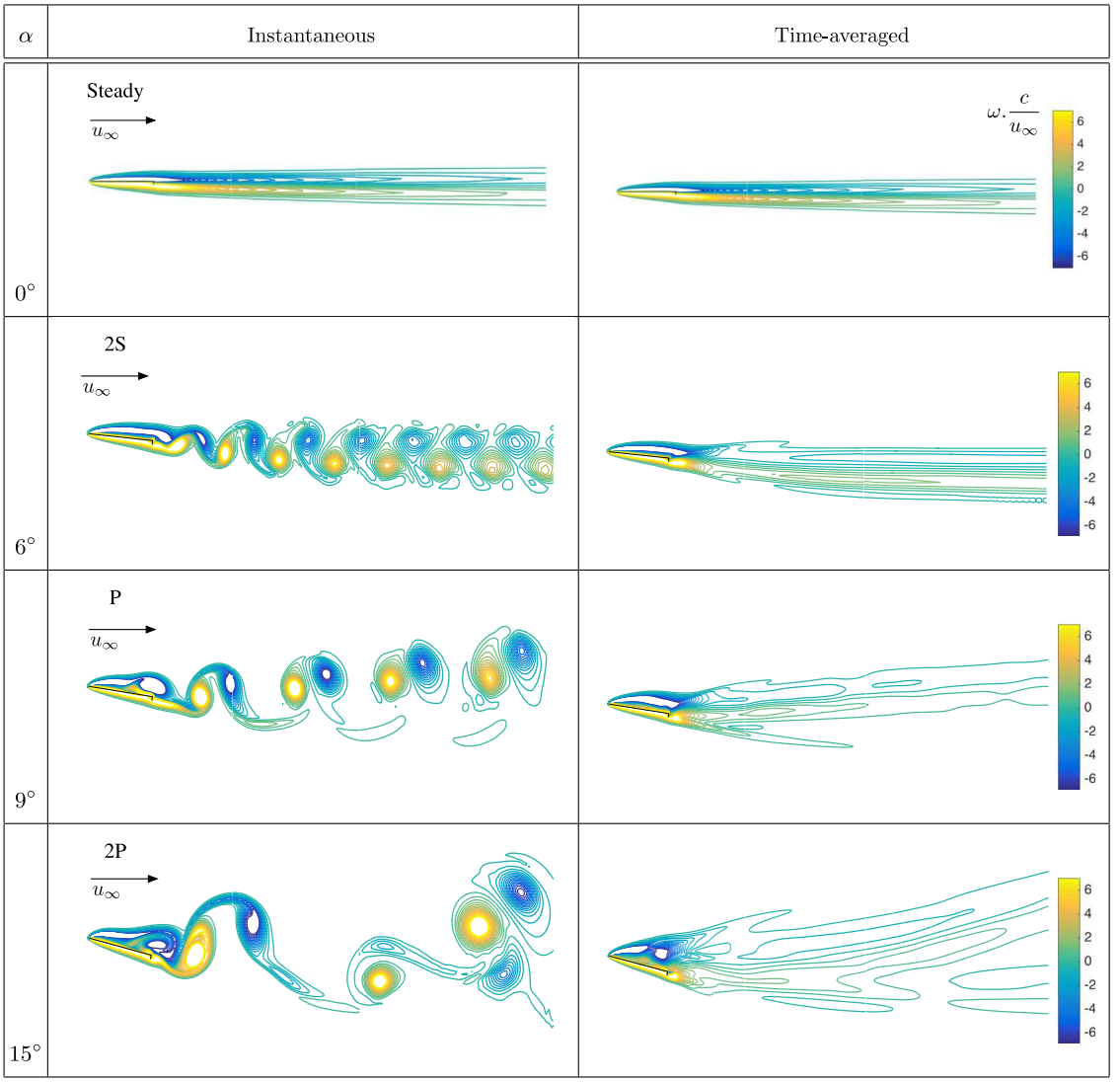

Fig. 2 Instantaneous and time-averaged two-dimensional vorticity fields $\omega c/u_\infty$, around NACA 0000 with a Gurney flap of $h/c = 0.06$ at various α; the contour plots represent the four characteristic regimes: steady, 2S, P, and 2P.

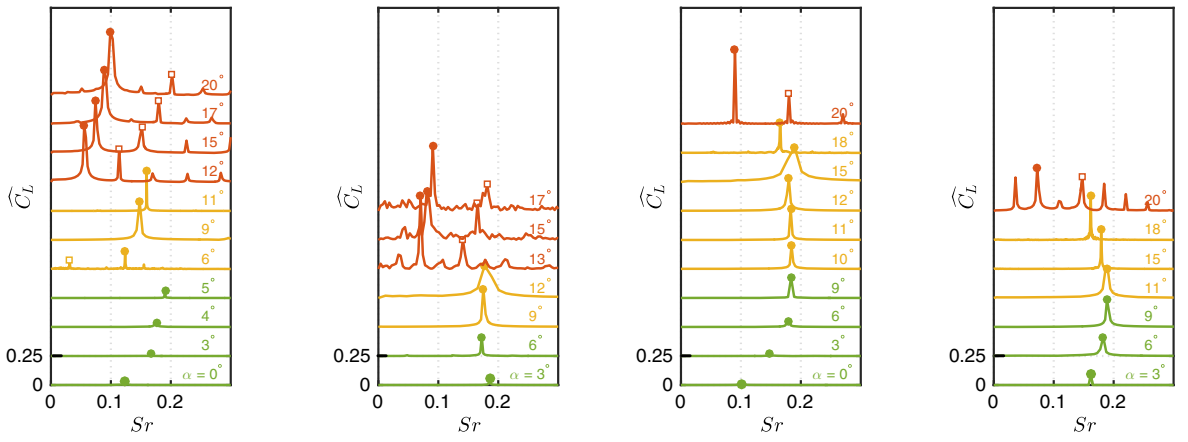

a) NACA 0000, *h/c* = 0.10 **b) NACA 0006, *h/c* = 0.15** **c) NACA 0012, *h/c* = 0.10** **d) NACA 0018, *h/c* = 0.15**

Fig. 3 Frequency spectra for a range of α for NACA 0000, 0006, 0012, and 0018 airfoils with Gurney flap; •, dominant vortex-shedding frequency; □, harmonic vortex-shedding frequency; regions with dominant $Sr \in [0.12,0.18]$ are classified as 2S and P regimes by the green and yellow regions, respectively, and $Sr \in [0.06,0.10]$ as 2P regime by the red region.

the flow. In fact, one should avoid operating an airfoil in such 2P regime in most cases, due to the large-scale unsteadiness. Nonetheless, we provide discussions on the wake dynamics and aerodynamic characteristics of the 2P mode in Secs. III.B and III.C to paint a complete description of the four wake regimes observed in two-dimensional flows.

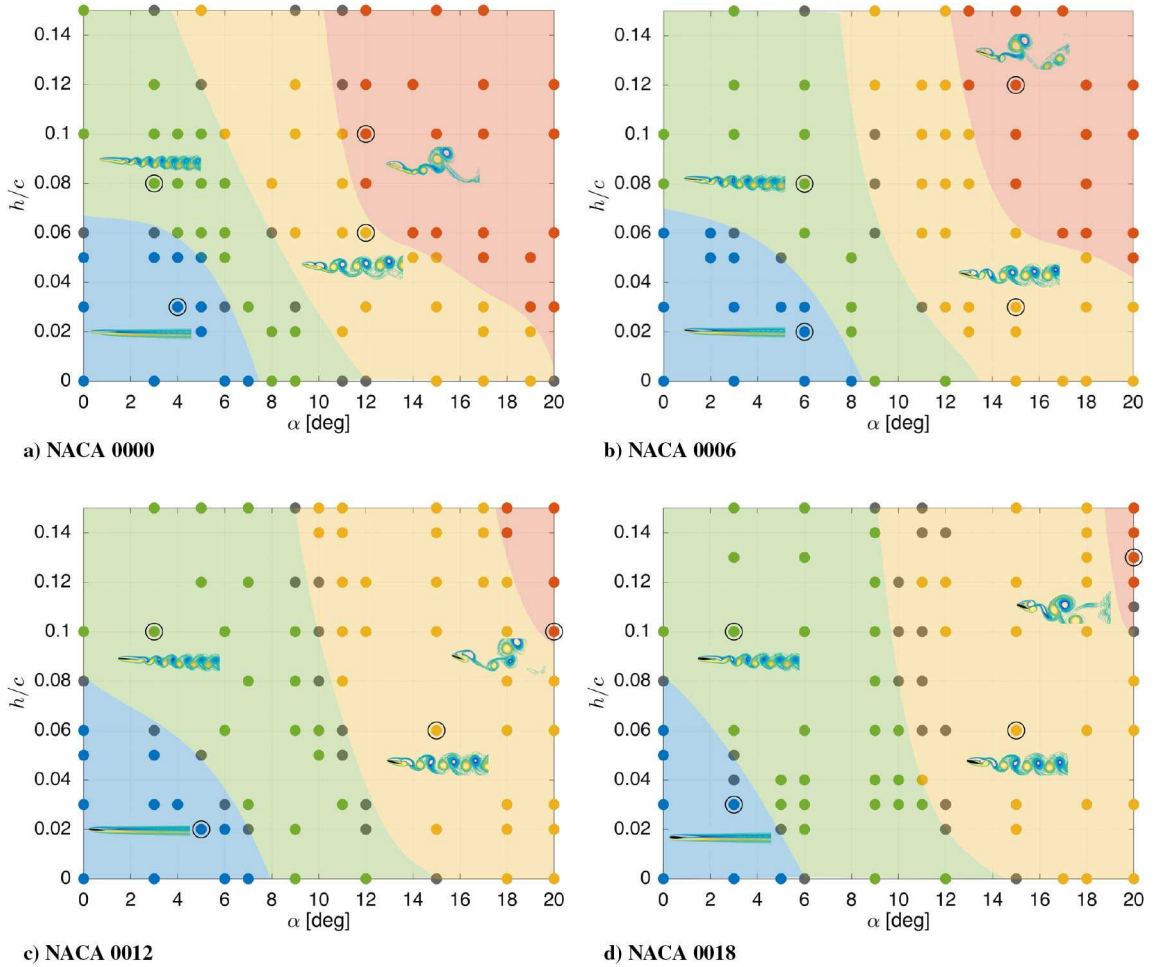

Fig. 4 Wake-classification diagram for NACA 0000, 0006, 0012, and 0018 airfoils are illustrated; all cases simulated in the current study are categorized into different characteristic wake regimes with respect to h/c and α values; different regimes are described by steady (blue), 2S (green), P (yellow), 2P (red), and transition between two regimes (gray); the boundaries for all the regimes are obtained by polynomial curve fitting.

We use the examination of the flow structure of the wake and the lift spectra to summarize the wake regimes of all four airfoils using a wake-classification diagram on the $(\alpha, h/c)$ plane. Figure 4 provides an overview of the simulations performed and the influence of the Gurney flap on the wake modes for different airfoils. The baseline cases without a flap are plotted on the x axis. Representative vorticity fields of different wake regimes observed are also portrayed for each airfoil case. With the addition of the Gurney flap, transition of the unsteady wake modes is shifted to lower angles of attack. The protruding flap disrupts the inflow, causing the flow to be unsteady at lower angles of attack. The wake-classification diagram shifts toward the left axis of the $(\alpha, h/c)$ plane with an increase in the Gurney-flap height.

When the airfoil geometry is changed from a flat plate to a thick airfoil, the occurrence of the 2P regime is delayed to higher h/c and α values. Furthermore, the size of the steady regime decreases. Increasing the thickness of the airfoil leads to a decrease in the influence of the Gurney flap as the thickness of the airfoil overshadows the effect of the flap. As a result of this, the complex 2P mode is revealed only at higher α and h/c values for thicker airfoils.

The wake-classification diagram provides a broad picture of the effect of adding a Gurney flap to the trailing edge of the airfoil. The diagram is useful to determine the nature of flow at different h/c and α values for all the airfoils studied. The overall performance of different airfoil Gurney-flap configurations can be understood from the diagram. This can be used to determine the optimal geometric and angle-of-attack conditions for different aerodynamic-performance requirements. Depending on the necessity, the ideal airfoil and corresponding Gurney-flap configuration can be chosen. In Sec. IV, we present insights from companion three-dimensional simulations and the influence of three-dimensionality on the wake dynamics.

B. Near-Wake Dynamics

Next, let us analyze the wake dynamics influencing the wake-mode transitions, which is responsible for the unsteady aerodynamic forces experienced by the airfoils. We, in particular, focus on the difference in shear-layer rollup and near-wake vortical structures that lead to the formation of vortices further downstream. Mainly three regions are examined in detail: suction and pressure sides of the airfoil, and vicinity of the Gurney flap. We depict the canonical near-field wake vortical structures analyzed herein in Fig. 5.

The main vortical structures observed at the near wake of the airfoil at different angles of attack and Gurney-flap heights are composed of the main clockwise rotating leading-edge vortex (LEV) on the suction side and the main counterclockwise rotating trailing-edge vortex (TEV) on the pressure side, visualized in Fig. 5a. Secondary LEV and TEV also shed from the airfoil at high angles of attack or with a large Gurney flap (in the 2P regime). Apart from these vortical structures, the formation of the secondary suction-side vortical structure with positive vorticity between the leading-edge separation and the suction-side wall, as shown in Fig. 5a, is observed to be important for the wake dynamics. The formation of this secondary structure is a result of the rollup of the large LEV caused by the separated flow. The formation and behavior of the structures vary with transition of the wake regime.

Let us present a brief summary of the near-wake dynamics, followed by specific details for each wake mode. The formation and periodic shedding of LEV and TEV are expected at moderate angles of attack for flow past an airfoil. Once a sufficiently strong LEV is formed, the secondary suction-side vortical structure emerges on the suction surface. The increase of circulation of the secondary vortical structure with a substantial increase of strength of the LEV is

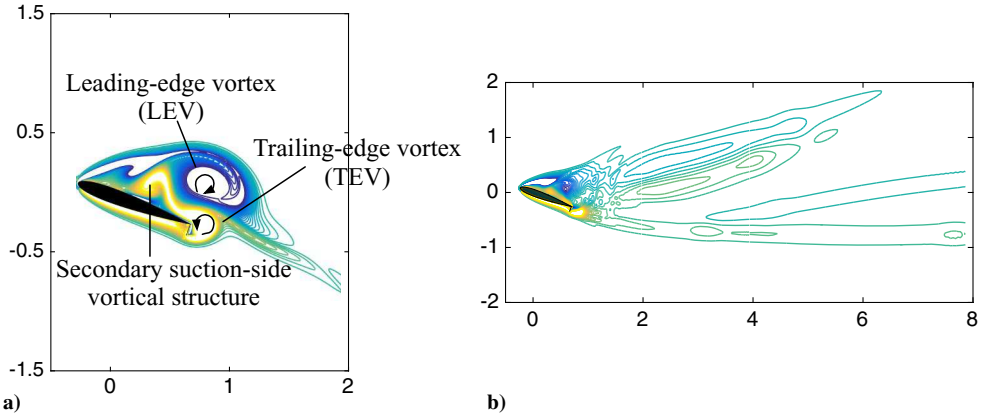

Fig. 5 Near-wake vortices for NACA 0012 with a Gurney flap of $h/c = 0.1$ at $\alpha = 20$ deg (2P wake regime): a) instantaneous vorticity field with 1) LEV, 2) TEV, and 3) secondary suction-side vortical structure; b) time-averaged vorticity field.

observed. Moreover, the strong influence of the LEV and the secondary vortical structure at higher α and h/c (in the 2P regime) causes the TEV to roll up onto the suction side, eventually leading to the transfer of vorticity from the secondary vortical structure to the TEV, as depicted in Fig. 5a. Note that the Gurney flap supports this merger by locally delaying the incoming flow as the TEV forms and merges with the secondary suction-side vortical structure. This phenomenon is observed only at very high angles of attack or with a substantially large Gurney flap, particularly in the 2P wake regime. The process results in a broader wake, leading to an increase in drag. Moreover, the mean flow is displaced upward with respect to the center of the wake, which is evident for the 2P mode from the time-averaged vorticity field in Fig. 5b, decreasing the lift enhancement.

For the 2S regime, Figs. 6a–6c, we observe the rollup and convection of a vortical structure with positive vorticity between the leading-edge separation and the suction-side wall, visible at the

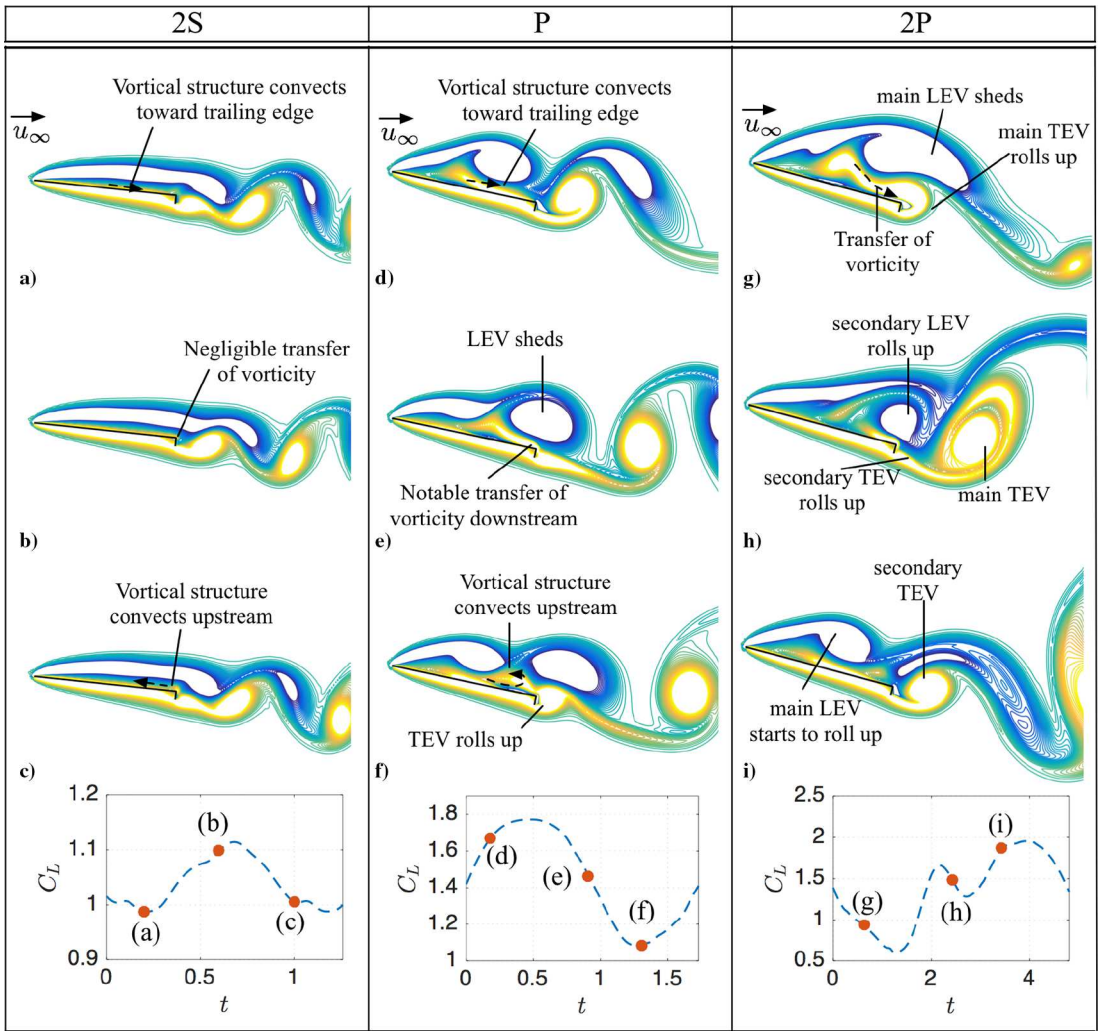

Fig. 6 Illustration of near-field flow of three cases classified under the a–c) 2S, d–f) P, and g–i) 2P regimes; the figure depicts instantaneous vorticity contour plots of flow over NACA 0000 airfoil at $\alpha = 6, 12$, and 15 deg with a Gurney flap of $h/c = 0.06$; corresponding instantaneous lift data, represented by ●, are also displayed on the bottom.

trailing edge in Fig. 5c. We refer to this vortical structure as the secondary suction-side vortical structure for the 2S regime. The circulation of the secondary suction-side vortical structure is small and is not strong enough to influence the TEV. The LEV and TEV shed periodically as single vortices, and there is no upward shift of the flow above the center of the wake. These are the reasons for the high lift-to-drag ratios, $\overline{C_L/C_D}$, observed for cases in the 2S wake mode, which are further described in Sec. III.C.

As the flow transitions to the P regime, Figs. 6d–6f, the circulation of the near-wake vortical structures increases. The strengthened LEV and secondary suction-side vortical structure influence the TEV to roll up along the outer walls of the Gurney flap with considerable transfer of vorticity from the secondary structure to the TEV. The LEV and TEV shed periodically, but a distinct vortex pair is formed compared to the individual vortices in the wake of the 2S regime. The wake width also increases and the flow shifts above the center of the wake. This leads to the increase in drag, decrease in lift enhancement, and fall of the $\overline{C_L/C_D}$ curve, as further discussed in Sec. III.C, for cases in the P regime.

In the 2P regime, Figs. 6g–6i, the circulation of the secondary suction-side vortical structure is sizable enough to influence the TEV to roll up onto the suction side, and the vorticity from the secondary vortical structure is transferred to the TEV. The transfer and accumulation of positive vorticity on the suction side cause the main LEV to shed, followed by the rollup of the leading-edge shear layer to form the second LEV. The main TEV sheds after a considerable buildup of circulation due to the transfer of vorticity from the secondary vortical structure. This leads to rollup of the second TEV on the pressure side. By the time the second LEV sheds from the trailing edge, the second TEV rolls up along the outer walls of the Gurney flap. The influence from the secondary vortical structure is not strong enough for the rollup of the second TEV onto the suction side. The second LEV convects downward, pairing up with the secondary TEV about $10c$ downstream. The wake width is increased considerably compared to the other unsteady regimes, with the flow shifting above and below the center of the wake. This wake dynamics lead to an increase of drag, a decrease of lift enhancement, and a degradation of the $\overline{C_L/C_D}$ curve, which are described in Sec. III.C.

C. Aerodynamic Forces

Next, we examine the effects of the wake modifications on the aerodynamic forces from the use of Gurney flaps. The main objective of attaching a Gurney flap to the trailing edge of an airfoil is to enhance the lift force experienced by the airfoil. The current results show that, at a low Reynolds number of $Re = 1.0 \times 10^3$, the Gurney flap is able to generate high levels of lift forces. It is also seen that, as the height of the flap is increased, the lift also increases. The lift coefficient C_L of representative cases for each airfoil is shown in Fig. 7, in which the time-averaged values $\overline{C_L}$ are depicted by the solid lines and the fluctuations in the forces are represented by the shaded regions. The blue lines for $h/c = 0.00$ cases depict the baseline results without a Gurney flap for all the airfoils.

As discussed earlier, $\overline{C_L}$ increases with α and h/c values for all airfoils. Lift-force enhancement of more than twice the baseline values is achieved using the Gurney flap, particularly at $h/c = 0.10$ for all airfoils in almost all cases. Because of the presence of the Gurney flap, an effective camber of the airfoil increases, attributing to lift enhancement. Fluctuations in the lift forces appear when the flow transitions from steady to unsteady state (2S regime). For a given angle of attack, $\overline{C_L}$ as well as the fluctuations of C_L are amplified with an increase in Gurney-flap height.

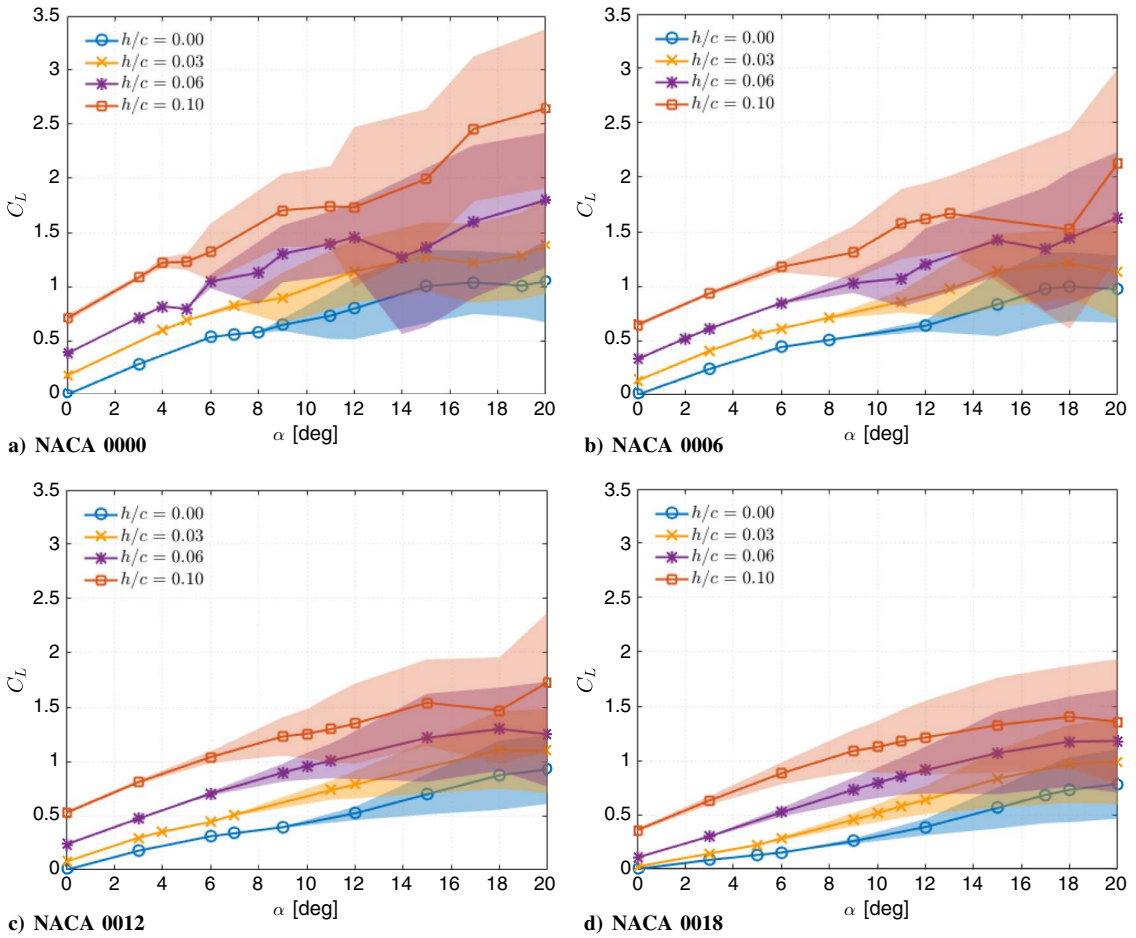

Fig. 7 Lift coefficient C_L over angle of attack α for NACA 0000, 0006, 0012, and 0018 airfoils with select Gurney-flap heights; the time-averaged $\overline{C_L}$ values are represented by the solid lines, and fluctuations in C_L are represented by the shaded region for each configuration.

At higher angles of attack, sudden jumps or bursts in C_L fluctuations are observed for all the cases. The fluctuations in C_L exhibit trends of sudden increase in magnitude with an increase in α, suggesting a transition from one flow regime to another with different Gurney-flap heights and angles of attack. The transitions correspond to the wake-mode shift from the 2S mode to the P mode, and then to the 2P mode. Thus, the airfoil experiences the highest magnitude of $\overline{C_L}$ as well as the fluctuations of C_L when the wake is classified under the 2P mode. Again, the transition of the wake from the steady regime through the 2P regime can be evidently observed by the jagged growth of C_L fluctuations with α for the NACA 0000 airfoil. The transition of the wake from the P to the 2P mode is clearly observed for the NACA 0006 and 0012 cases at high angles of attack.

The benefit of lift enhancement is, however, accompanied with a penalty of some drag increase. The drag coefficients C_D of representative cases for each airfoil are shown in Fig. 8. As it can be observed, $\overline{C_D}$ increases with α and h/c values. The $\overline{C_D}$ for all cases have low values at lower angles of attack. The appearance of fluctuations in C_D in conjunction with the wake transition from the steady regime to the 2S regime is also observed at lower α, but the magnitudes of the fluctuations are small. Also, the sudden and jagged variations in the fluctuations of C_D with an increase in α are small compared to that observed for the C_L fluctuations. The fluctuations in C_D increase suddenly at high angles of attack when the wake transitions from the P mode to the 2P mode, also observed above for the lift, for all airfoils.

The thickness of the airfoil plays a major role on the aerodynamic forces experienced by the airfoil. With an increase in airfoil thickness, the effect of the Gurney flap is overshadowed. As a result, different trends are observed for the lift and drag on the airfoils. For the range of angles of attack considered in this study, the magnitudes of $\overline{C_L}$ and fluctuations in C_L decrease for thicker airfoils. Whereas the drag force increases with airfoil thickness at low angles of attack, which is expected for the baseline cases, the trend reverses at higher angles of attack, and the drag generated decreases for thicker airfoils compared to thinner airfoils. Another behavior observed is for the lift and drag slopes. The lift slope, $a = \mathrm{d}\overline{C_L}/\mathrm{d}\alpha$, follows a jagged trend for thinner airfoils, whereas the slope is smoother for thicker airfoils. The same is observed for the drag slope, although the fluctuations of the drag slope for thinner airfoils are small compared to that of the lift slope. All the aforementioned observations further emphasize the reduced influence from the Gurney flap due to the overshadowing effect of the airfoil thickness.

The lift-to-drag ratio, $\overline{C_L/C_D}$, for all airfoils is examined and depicted in Fig. 9. With an increase in α, the $\overline{C_L/C_D}$ increases drastically, reaching its maximum value, and then decreases gradually. The significant enhancement of $\overline{C_L/C_D}$ is achieved with the utilization of a Gurney flap. The $\overline{C_L/C_D}$ at lower angles of attack, in the range of $\alpha \in [0, 12]$ deg, is observed to be higher compared to the baseline cases in general for all airfoils and flap heights. This range of α is smaller for thinner airfoils (NACA 0000 and 0006), although the peak value of $\overline{C_L/C_D}$ is higher compared to thicker airfoils (NACA 0012 and 0018). This range of α corresponds to the steady and 2S regime for all the airfoils, where the drag remains low. At a higher range of α, the $\overline{C_L/C_D}$ decreases and reaches values close to the baseline values for the controlled cases of all airfoils. This range of α corresponds to the P and 2P regimes of the respective airfoils where the highest magnitude of drag is experienced by the airfoils. The $\overline{C_L/C_D}$ curves degrade below the baseline cases for NACA 0000 and 0006 at higher α.

All the aforementioned observations show that an airfoil with a large Gurney flap at high angles of attack experiences large forces. With an increase in α, thinner airfoils (NACA 0000 and 0006) experience the highest increase in lift and drag, whereas thicker

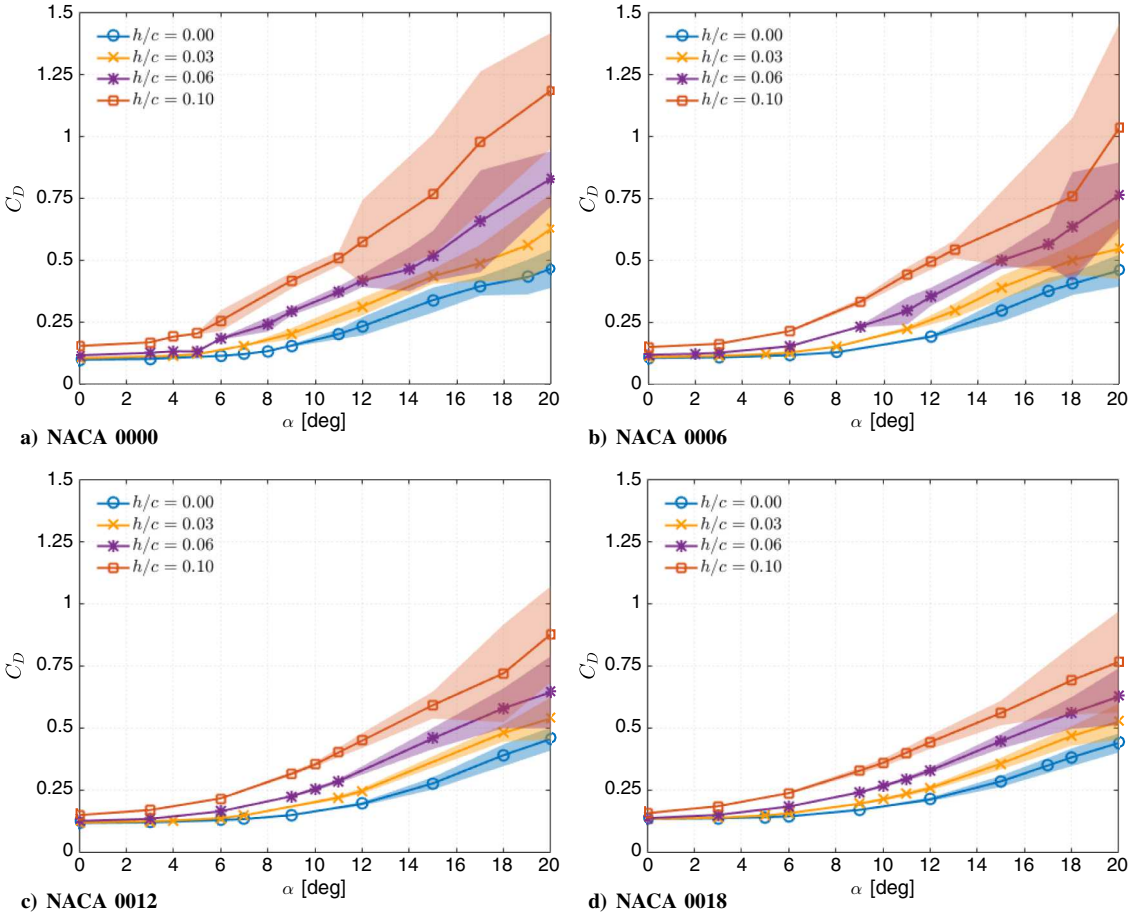

Fig. 8 Drag coefficient C_D over angle of attack α for NACA 0000, 0006, 0012, and 0018 airfoils with select Gurney-flap heights; the time-averaged $\overline{C_D}$ values are represented by the solid lines, and fluctuations in C_D are represented by the shaded region for each configuration.

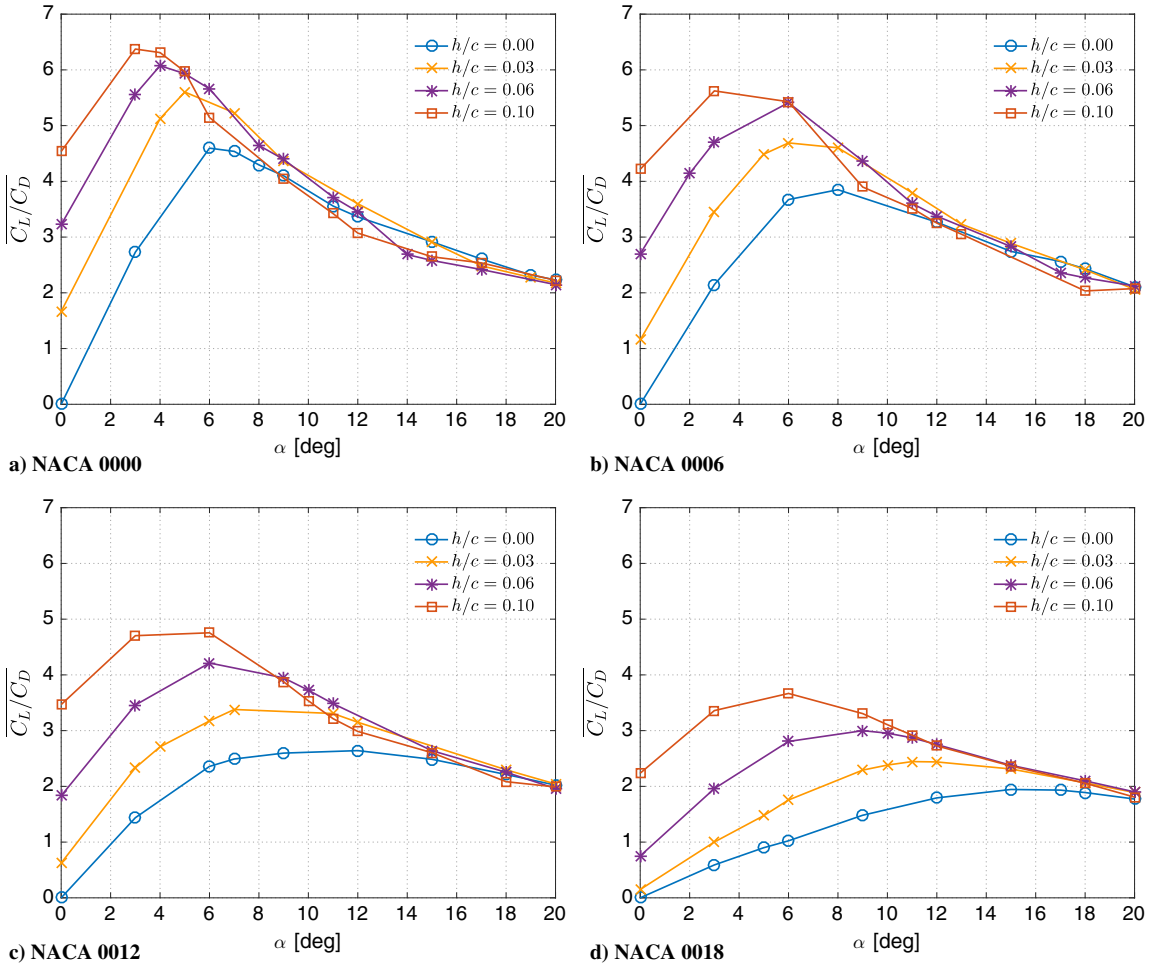

Fig. 9 Lift-to-drag ratio $\overline{C_L/C_D}$ over angle of attack α for NACA 0000, 0006, 0012, and 0018 airfoils with Gurney flap.

airfoils (NACA 0012 and 0018) attribute with smoother lift and drag slopes. The enhanced lift-to-drag ratio brought about by the Gurney flap is maintained over a wider range of α and h/c values in thicker airfoils, whereas thinner airfoils experience higher magnitude of $\overline{C_L/C_D}$ over a narrower range of α. Thus, for high levels of lift generation and $\overline{C_L/C_D}$ requirements, thinner airfoils can be suitable among the considered airfoils. In contrast, to obtain the enhanced $\overline{C_L/C_D}$ over a wider range of angles of attack and lower drag when a Gurney flap is attached, thicker airfoils perform well, although with a relatively lower magnitude of $\overline{C_L/C_D}$.

IV. Analysis of Three-Dimensional Flows

A three-dimensional analysis is performed on the flow around the NACA 0006 airfoil with a Gurney flap of $h/c = 0.08$ at $\alpha = 6, 12$, and 18 deg to examine the spanwise effects on the wakes. The chosen angles of attack yield the 2S, P, and 2P wake regimes, respectively, for a two-dimensional flow, as shown in Fig. 4b. The three-dimensional flowfields and the resulting force characteristics are summarized in Fig. 10. We use the isosurface of the Q criterion [65] to visualize the three-dimensional airfoil wake. The aerodynamic force characteristics of the three-dimensional flow are also compared to those obtained from the two-dimensional analysis.

The cases with $\alpha = 6$ and 12 deg, classified as the 2S and P wakes, respectively, in a two-dimensional flow, remain two dimensional with a spanwise extension of the airfoil. Although the 12 deg case shows some spanwise variations in the flow, it can be considered as nominally two dimensional. The instantaneous snapshots of the two cases show the presence of the alternating positive and negative vortices leading to the formation of the von Kármán vortex street, previously observed in the two-dimensional analysis. The time-averaged flowfield also corresponds to that observed for a von Kármán wake, and previously observed in the two-dimensional analysis. These observations suggest that the dominant vortex-shedding frequency, lift and drag forces, and the lift-to-drag ratio experienced by the airfoil are similar to those observed in the two-dimensional analysis. This is noted from the similarity in the aerodynamic force characteristics for the two-dimensional and three-dimensional results in Fig. 10, further highlighting the two-dimensional nature of the flow. The same criteria used in the two-dimensional analysis are applied to classify the $\alpha = 6$ and 12 deg cases under the 2S and P wake regimes.

The case with $\alpha = 18$ deg, classified under the 2P regime for a two-dimensional flow, is influenced by the spanwise instabilities in the flow and results in a fully three-dimensional flow with an underlying von Kármán wake. The formation of the 2P wake mode is not observed. The 2P wake structure is disrupted by the spanwise instabilities, and the wake structure is suppressed to a von Kármán vortex street with spanwise variations. As seen from the top view of Fig. 10, the cores of the positive and negative vortices in the von Kármán street also show spanwise variations. The time-averaged flowfield depicts the reduction in the wake thickness considerably compared to that observed in the two-dimensional 2P wake structure (see Fig. 2). This reflects in considerable reduction in the drag force experienced by the airfoil compared to that for the two-dimensional 2P regime. The altered dynamics of the shear-layer rollup leads to a reduction in the lift force compared to the two-dimensional 2P case. These inferences are observed from the aerodynamic force characteristics of the $\alpha = 18$ deg case in Fig. 10. The considerable decrease in the drag force compensates for the reduction in the lift enhancement experienced by the airfoil to maintain the lift-to-drag ratio. The dominant shedding frequency of $Sr = 0.155$, similar to the values observed for that of the 2S and P wake structures, substantiates the von Kármán wake behavior for the dominant vortical structures of the three-dimensional flowfield.

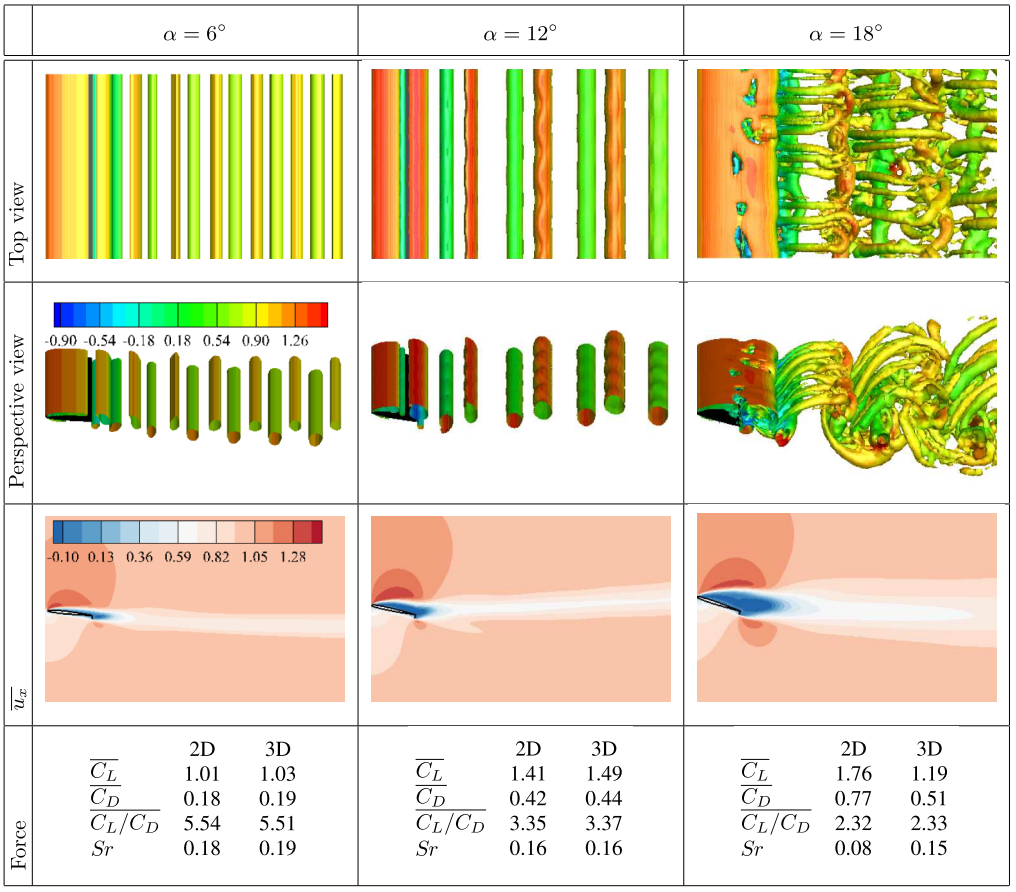

Fig. 10 Flow visualization and aerodynamic force characteristics of flow over the NACA 0006 airfoil with Gurney flap of $h/c = 0.08$ at $\alpha = 6$,12, and 18 deg with three-dimensional DNS; each row consists of the top and perspective views of instantaneous snapshots of the Q criterion [65] isosurface colored with u_x, the time-averaged $\overline{u_x}$, and the comparison of aerodynamic force characteristics between the respective cases of two-dimensional and three-dimensional analyses.

We have observed that the two-dimensional analysis provides a foundation to understand the occurrence of the 2S and P wake regimes for the three-dimensional spanwise-periodic setup. The deviation with three-dimensional flow appears for the fully three-dimensional flow for what would be the 2P wake regime in the two-dimensional setting. Nonetheless, it should be noted that, at a higher Reynolds number, the three-dimensionality of the wake structures can be instigated to even the flow classified as two-dimensional wake regimes at this Reynolds number. This transition of the flowfield of each particular wake regime from two dimensional to three dimensional is beyond the scope of the current work, and the readers are referred to studies that focus in such analyses [51,66,67]. Further analyses have to be performed to completely understand these effects for the current problem. The novelty of the current work is in understanding the transition of the wake regimes from steady through 2P or von Kármán vortex street having spanwise variations with change in different parameters of airfoil thickness, angle of attack, effects of the Gurney flap and the flap height, and associated effects on the force characteristics of the airfoil in an incompressible flow at $Re = 1.0 \times 10^3$.

V. Conclusions

A large number of two-dimensional direct numerical simulations for incompressible flow have been performed over different airfoils —NACA 0000 (flat plate), 0006, 0012, and 0018—at $Re = 1.0 \times 10^3$ with and without a Gurney flap attached to the trailing edge over a range of angles of attack. The use of the Gurney flap significantly enhances the lift experienced by the airfoils. Lift-to-drag ratio increase exceeding twice that of the baseline cases are observed with the attachment of the Gurney flap. However, the benefit of lift enhancement is accompanied with a penalty of drag increase, particularly at high angles of attack. This further leads to degradation of the lift-to-drag ratios below baseline cases at high angles of attack, although high-lift enhancement is also observed at these flow conditions. The overshadowing effect of thicker airfoils on the Gurney flap reduces the influence of the flap on flow modification in such airfoils. The aerodynamic forces experienced by these airfoils are also significantly altered compared to that for thinner airfoils. Even though the magnitude of the lift and lift-to-drag-ratio enhancement is reduced for thicker airfoils, the lift and drag slopes are much smoother and the drag is also reduced at higher angles of attack.

Analyzing the lift spectra and flow structure of the airfoil wake reveals the presence of different vortex-shedding patterns in the wake. These are classified into four wake regimes: 1) steady, 2) 2S (periodic von Kármán vortex shedding of alternating counterclockwise and clockwise rotating vortices), 3) P (periodic von Kármán shedding of a single vortex pair), and 4) 2P (periodic shedding of two distinct vortex pairs). Characteristic Strouhal number corresponding to the vortex-shedding phenomenon is also observed for each of the wake modes. The detailed analysis of the near-wake properties also revealed the wake-mode transitions. Among the different vortical structures formed in the near wake of the airfoils, the observations suggest that the strong LEV and the secondary vortical structure with counterclockwise direction of vorticity formed on the suction side of the airfoil lead to the rollup of the TEV onto the suction side at high angles of attack and Gurney-flap heights. This leads to the emergence of different vortex-shedding patterns and, hence, the wake-mode transitions. A selected number of three-dimensional DNS of representative cases have also been performed to analyze the three-dimensional effects on these wake-mode transitions in a spanwise periodic setting. The results suggest that the 2S and P wake modes tend to remain two dimensional

even with spanwise effects, although the flow presents three-dimensionality at very high angles of attack at this $Re = 1.0 \times 10^3$. For a three-dimensional flow, the 2P mode is suppressed by the spanwise instabilities reducing to a von Kármán vortex street like wake structure, suggesting the need for a careful three-dimensional analysis.

The existence of the wake modes is summarized in a wake-classification diagram over a wide range of angles of attack and Gurney-flap heights for each of the airfoils. Unsteady wake regimes appear at lower angles of attack with the addition of the Gurney flap. The wake-classification diagram provides guidance on the implementation of the Gurney flap at different conditions for the required aerodynamic performance, motivating studies in passive as well as active Gurney flaps. The airfoil performance can be assessed depending on the nature of the wake regime the respective flow is classified under for the particular angle of attack and flap height.

Acknowledgments

Muralikrishnan Gopalakrishnan Meena and Kunihiko Taira were partially supported by the National Science Foundation (award number 1632003). The authors thank the insightful discussions with Phillip Munday, Chi-An Yeh, and Daisuke Oshiyama. The majority of the computation for this project was performed at the Research Computing Center at the Florida State University.

References

[1] Mueller, T. J., *Fixed and Flapping Wing Aerodynamics for Micro Air Vehicle Applications*, Vol. 195, AIAA, Reston, VA, 2001.

[2] Mueller, T. J., and DeLaurier, J. D., "Aerodynamics of Small Vehicles," *Annual Review of Fluid Mechanics*, Vol. 35, No. 1, 2003, pp. 89–111. doi:10.1146/annurev.fluid.35.101101.161102

[3] Pines, D. J., and Bohorquez, F., "Challenges Facing Future Micro-Air-Vehicle Development," *Journal of Aircraft*, Vol. 43, No. 2, 2006, pp. 290–305. doi:10.2514/1.4922

[4] Dickinson, M. H., and Gotz, K. G., "Unsteady Aerodynamic Performance of Model Wings at Low Reynolds Numbers," *Journal of Experimental Biology*, Vol. 174, No. 1, 1993, pp. 45–64.

[5] Ellington, C. P., Van Den Berg, C., Willmott, A. P., and Thomas, A. L., "Leading-Edge Vortices in Insect Flight," *Nature*, Vol. 384, No. 6610, 1996, pp. 626–630. doi:10.1038/384626a0

[6] Triantafyllou, M. S., Triantafyllou, G., and Yue, D., "Hydrodynamics of Fishlike Swimming," *Annual Review of Fluid Mechanics*, Vol. 32, No. 1, 2000, pp. 33–53. doi:10.1146/annurev.fluid.32.1.33

[7] Trizila, P., Kang, C.-K., Aono, H., Shyy, W., and Visbal, M., "Low-Reynolds-Number Aerodynamics of a Flapping Rigid Flat Plate," *AIAA Journal*, Vol. 49, No. 4, 2011, pp. 806–823. doi:10.2514/1.J050827

[8] Fujita, K., Nagai, H., and Asai, K., "Conceptual Design of a Miniature, Propeller-Driven Airplane for Mars," AIAA Paper 2012-0847, Jan. 2012.

[9] Suwa, T., Nose, K., Numata, D., Nagai, H., and Asai, K., "Compressibility Effects on Airfoil Aerodynamics at Low Reynolds Number," AIAA Paper 2012-3029, June 2012.

[10] Nagai, H., Asai, K., Numata, D., Suwa, T., and Anyoji, M., "Characteristics of Low-Reynolds Number Airfoils in a Mars Wind Tunnel," AIAA Paper 2013-0073, Jan. 2013.

[11] Yonezawa, K., Goto, Y., Sunada, S., Hayashida, T., Suwa, T., Sakai, N., Nagai, H., Asai, K., and Tsujimoto, Y., "An Investigation of Airfoils for Development of a Propeller of Mars Exploration Airplane," *Journal of the Japan Society for Aeronautical and Space Science*, Vol. 62, No. 1, 2014, pp. 24–30. doi:10.2322/jjsass.62.24

[12] Munday, P. M., Taira, K., Suwa, T., Numata, D., and Asai, K., "Nonlinear Lift on a Triangular Airfoil in Low-Reynolds-Number Compressible Flow," *Journal of Aircraft*, Vol. 52, No. 3, 2015, pp. 924–931. doi:10.2514/1.C032983

[13] Garmann, D. J., and Visbal, M. R., "Numerical Investigation of Transitional Flow over a Rapidly Pitching Plate," *Physics of Fluids*, Vol. 23, No. 9, 2011, Paper 094106. doi:10.1063/1.3626407

[14] Taira, K., and Colonius, T., "Three-Dimensional Flows Around Low-Aspect-Ratio Flat-Plate Wings at Low Reynolds Numbers," *Journal of Fluid Mechanics*, Vol. 623, March 2009, pp. 187–207. doi:10.1017/S0022112008005314

[15] Pitt Ford, C. W., and Babinsky, H., "Lift and the Leading-Edge Vortex," *Journal of Fluid Mechanics*, Vol. 720, April 2013, pp. 280–313. doi:10.1017/jfm.2013.28

[16] Mancini, P., Manar, F., Granlund, K., Ol, M. V., and Jones, A. R., "Unsteady Aerodynamic Characteristics of a Translating Rigid Wing at Low Reynolds Number," *Physics of Fluids*, Vol. 27, No. 12, 2015, Paper 123102. doi:10.1063/1.4936396

[17] DeVoria, A. C., and Mohseni, K., "On the Mechanism of High-Incidence Lift Generation for Steadily Translating Low-Aspect-Ratio Wings," *Journal of Fluid Mechanics*, Vol. 813, Feb. 2017, pp. 110–126. doi:10.1017/jfm.2016.849

[18] Edstrand, A. M., Davis, T. B., Schmid, P. J., Taira, K., and Cattafesta, L. N., "On the Mechanism of Trailing Vortex Wandering," *Journal of Fluid Mechanics*, Vol. 801, Aug. 2016, pp. R1–R11. doi:10.1017/jfm.2016.440

[19] Lissaman, P., "Low-Reynolds-Number Airfoils," *Annual Review of Fluid Mechanics*, Vol. 15, No. 1, 1983, pp. 223–239. doi:10.1146/annurev.fl.15.010183.001255

[20] Percy, T., Bright, E., and Torres, A., "Assessing the Relative Risk of Aerocapture Using Probabilistic Risk Assessment," AIAA Paper 2005-4107, July 2005.

[21] Carr, L. W., "Progress in Analysis and Prediction of Dynamic Stall," *Journal of Aircraft*, Vol. 25, No. 1, 1988, pp. 6–17. doi:10.2514/3.45534

[22] Leishman, G., *Principles of Helicopter Aerodynamics*, 2nd ed., Cambridge Univ. Press, New York, 2006.

[23] Chen, K. K., Colonius, T., and Taira, K., "The Leading-Edge Vortex and Quasisteady Vortex Shedding on an Accelerating Plate," *Physics of Fluids*, Vol. 22, March 2010, Paper 033601.

[24] Ozen, C. A., and Rockwell, D., "Three-Dimensional Vortex Structure on a Rotating Wing," *Journal of Fluid Mechanics*, Vol. 707, Sept. 2012, pp. 541–550. doi:10.1017/jfm.2012.298

[25] Jantzen, R. T., Taira, K., Granlund, K., and Ol, M. V., "Vortex Dynamics Around Pitching Plates," *Physics of Fluids*, Vol. 26, No. 5, 2014, Paper 053696. doi:10.1063/1.4879035

[26] Jones, A. R., Medina, A., Spooner, H., and Mulleners, K., "Characterizing a Burst Leading-Edge Vortex on a Rotating Flat Plate Wing," *Experiments in Fluids*, Vol. 57, No. 4, 2016, pp. 1–16. doi:10.1007/s00348-016-2143-7

[27] Owen, T., Biemann, K., Rushneck, J., Biller, J. E., Howarth, D. W., and Lafleur, A. L., "The Composition of the Atmosphere at the Surface of Mars," *Journal of Geophysical Research*, Vol. 82, No. 28, 1977, pp. 4635–4639. doi:10.1029/JS082i028p04635

[28] Seiff, A., and Kirk, D. B., "Structure of the Atmosphere of Mars in Summer at Mid-Latitudes," *Journal of Geophysical Research*, Vol. 82, No. 28, 1977, pp. 4364–4378. doi:10.1029/JS082i028p04364

[29] Anyoji, M., Numata, D., Nagai, H., and Asai, K., "Effects of Mach Number and Specific Heat Ratio on Low-Reynolds-Number Airfoil Flows," *AIAA Journal*, Vol. 53, No. 6, 2015, pp. 1640–1654. doi:10.2514/1.J053468

[30] Seifert, A., Greenblatt, D., and Wygnanski, I. J., "Active Separation Control: An Overview of Reynolds and Mach Numbers Effects," *Aerospace Science and Technology*, Vol. 8, No. 7, 2004, pp. 569–582. doi:10.1016/j.ast.2004.06.007

[31] Greenblatt, D., and Wygnanski, I., "The Control of Flow Separation by Periodic Excitation," *Progress in Aerospace Science*, Vol. 36, No. 7, 2000, pp. 487–545. doi:10.1016/S0376-0421(00)00008-7

[32] Little, J., Nishihara, M., Adamovich, I., and Samimy, M., "High-Lift Airfoil Trailing Edge Separation Control Using a Single Dielectric Barrier Discharge Plasma Actuator," *Experiments in Fluids*, Vol. 48, No. 3, 2010, pp. 521–537. doi:10.1007/s00348-009-0755-x

[33] Whalen, E. A., Lacy, D. S., Lin, J. C., Andino, M. Y., Washburn, A. E., Graff, E. C., and Wygnanski, I. J., "Performance Enhancement of a Full-Scale Vertical Tail Model Equipped with Active Flow Control," AIAA Paper 2015-0784, Jan. 2015.

[34] Yeh, C.-A., Munday, P., and Taira, K., "Use of Local Periodic Heating for Separation Control on a NACA 0012 Airfoil," AIAA Paper 2017-1451, Jan. 2017.
[35] Munday, P. M., and Taira, K., "On the Lock-on of Vortex Shedding to Oscillatory Actuation Around a Circular Cylinder," *Physics of Fluids*, Vol. 25, No. 1, 2013, pp. 1–13. doi:10.1063/1.4772977
[36] Taira, K., and Colonius, T., "Effect of Tip Vortices in Low-Reynolds-Number Poststall Flow Control," *AIAA Journal*, Vol. 47, No. 3, 2009, pp. 749–756. doi:10.2514/1.40615
[37] Taira, K., Rowley, C. W., Colonius, T., and Williams, D. R., "Lift Enhancement for Low-Aspect-Ratio Wings with Periodic Excitation," *AIAA Journal*, Vol. 48, No. 8, 2010, pp. 1785–1790. doi:10.2514/1.J050248
[38] Taira, K., Rowley, C. W., and Colonius, T., "Lock-on to a High-Lift State with Oscillatory Forcing in a Three-Dimensional Wake Flow," *Active Flow Control II*, Springer, Berlin, 2010, pp. 81–93.
[39] Liebeck, R. H., "Design of Subsonic Airfoils for High Lift," *Journal of Aircraft*, Vol. 15, No. 9, 1978, pp. 547–561. doi:10.2514/3.58406
[40] Katz, J., and Largman, R., "Effect of 90 Degree Flap on the Aerodynamics of a Two Element Airfoil," *Journal of Fluids Engineering*, Vol. 111, No. 1, 1989, pp. 93–94. doi:10.1115/1.3243605
[41] Neuhart, D. H., and Pendergraft, O. C., Jr., "A Water Tunnel Study of Gurney Flaps," NASA TM 4071, 1988.
[42] Jeffrey, D., Zhang, X., and Hurst, D. W., "Aerodynamics of Gurney Flaps on a Single-Element High-Lift Wing," *Journal of Aircraft*, Vol. 37, No. 2, 2000, pp. 295–301. doi:10.2514/2.2593
[43] Li, Y., Wang, J., and Zhang, P., "Effects of Gurney Flaps on a NACA0012 Airfoil," *Flow, Turbulence and Combustion*, Vol. 68, No. 1, 2002, pp. 27–39. doi:10.1023/A:1015679408150
[44] Oshiyama, D., Numata, D., and Asai, K., "Lift-Enhancing Mechanism of Mini Flaps at Low-Reynolds Number," Japan Soc. for Aeronautical and Space Science Paper 2015-D12-1087, 2015.
[45] Zhang, P., Liu, A., and Wang, J., "Aerodynamic Modification of NACA 0012 Airfoil by Trailing-Edge Plasma Gurney Flap," *AIAA Journal*, Vol. 47, No. 10, 2009, pp. 2467–2474. doi:10.2514/1.43379
[46] Feng, L.-H., Choi, K.-S., and Wang, J.-J., "Flow Control over an Airfoil Using Virtual Gurney Flaps," *Journal of Fluid Mechanics*, Vol. 767, March 2015, pp. 595–626. doi:10.1017/jfm.2015.22
[47] Mittal, S., and Tezduyar, T. E., "Massively Parallel Finite Element Computation of Incompressible Flows Involving Fluid–Body Interactions," *Computer Methods in Applied Mechanics and Engineering*, Vol. 112, Nos. 1–4, 1994, pp. 253–282. doi:10.1016/0045-7825(94)90029-9
[48] Kurtulus, D. F., "On the Unsteady Behavior of the Flow Around NACA 0012 Airfoil with Steady External Conditions at $Re = 1000$," *International Journal of Micro Air Vehicles*, Vol. 7, No. 3, 2015, pp. 301–326.10.1260/1756-8293.7.3.301
[49] Kurtulus, D. F., "On the Wake Pattern of Symmetric Airfoils for Different Incidence Angles at $Re = 1000$," *International Journal of Micro Air Vehicles*, Vol. 8, No. 2, 2016, pp. 109–139. doi:10.1177/1756829316653700
[50] Mateescu, D., Panahi, A., and Roy, V., "Analysis of the Flow Past Airfoils with Gurney Flaps at Low Reynolds Numbers," AIAA Paper 2014-0040, Jan. 2014.
[51] Hoarau, Y., Braza, M., Ventikos, Y., Faghani, D., and Tzabiras, G., "Organized Modes and the Three-Dimensional Transition to Turbulence in the Incompressible Flow Around a NACA0012 Wing," *Journal of Fluid Mechanics*, Vol. 496, Dec. 2003, pp. 63–72. doi:10.1017/S0022112003006530
[52] Suzuki, T., Ji, H., and Yamamoto, F., "Unsteady PTV Velocity Field Past an Airfoil Solved with DNS, Part 1: Algorithm of Hybrid Simulation and Hybrid Velocity Field at $Re \approx 10^3$," *Experiments in Fluids*, Vol. 47, No. 6, 2009, pp. 977–994. doi:10.1007/s00348-009-0692-8
[53] Liu, Y., Li, K., Zhang, J., Wang, H., and Liu, L., "Numerical Bifurcation Analysis of Static Stall of Airfoil and Dynamic Stall Under Unsteady Perturbation," *Communications in Nonlinear Science and Numerical Simulation*, Vol. 17, No. 8, 2012, pp. 3427–3434. doi:10.1016/j.cnsns.2011.12.007
[54] Taira, K., and Colonius, T., "The Immersed Boundary Method: A Projection Approach," *Journal of Computational Physics*, Vol. 225, No. 2, 2007, pp. 2118–2137. doi:10.1016/j.jcp.2007.03.005
[55] Colonius, T., and Taira, K., "A Fast Immersed Boundary Method Using a Nullspace Approach and Multi-Domain Far-Field Boundary Conditions," *Computer Methods in Applied Mechanics and Engineering*, Vol. 197, Nos. 25–28, 2008, pp. 2131–2146. doi:10.1016/j.cma.2007.08.014
[56] Ham, F., and Iaccarino, G., "Energy Conservation in Collocated Discretization Schemes on Unstructured Meshes," *Annual Research Briefs*, Vol. 2004, 2004, pp. 3–14.
[57] Ham, F., Mattsson, K., and Iaccarino, G., "Accurate and Stable Finite Volume Operators for Unstructured Flow Solvers," *Annual Research Briefs*, 2006, pp. 243–261.
[58] Morinishi, Y., Lund, T. S., Vasilyev, O. V., and Moin, P., "Fully Conservative Higher Order Finite Difference Schemes for Incompressible Flow," *Journal of Computational Physics*, Vol. 143, No. 1, 1998, pp. 90–124. doi:10.1006/jcph.1998.5962
[59] Kim, J., and Moin, P., "Application of a Fractional-Step Method to Incompressible Navier–Stokes Equations," *Journal of Computational Physics*, Vol. 59, No. 2, 1985, pp. 308–323. doi:10.1016/0021-9991(85)90148-2
[60] Williamson, C. H. K., and Roshko, A., "Vortex Formation in the Wake of an Oscillating Cylinder," *Journal of Fluids and Structures*, Vol. 2, No. 4, 1988, pp. 355–381. doi:10.1016/S0889-9746(88)90058-8
[61] Ongoren, A., and Rockwell, D., "Flow Structure from an Oscillating Cylinder, Part 2: Mode Competition in the Near Wake," *Journal of Fluid Mechanics*, Vol. 191, June 1988, pp. 225–245. doi:10.1017/S0022112088001570
[62] Brika, D., and Laneville, A., "Vortex-Induced Vibrations of a Long Flexible Circular Cylinder," *Journal of Fluid Mechanics*, Vol. 250, May 1993, pp. 481–481. doi:10.1017/S0022112093001533
[63] Koochesfahani, M. M., "Vortical Patterns in the Wake of an Oscillating Airfoil," *AIAA Journal*, Vol. 27, No. 9, 1989, pp. 1200–1205. doi:10.2514/3.10246
[64] Jones, K., Dohring, C., and Platzer, M., "Wake Structures Behind Plunging Airfoils: A Comparison of Numerical and Experimental Results," AIAA Paper 1996-0078, Jan. 1996.
[65] Hunt, J. C. R., Wray, A. A., and Moin, P., "Eddies, Stream, and Convergence Zones in Turbulent Flows," Center for Turbulence Research, CTR-S88, Stanford Univ., CA, 1988.
[66] Freymuth, P., "On Transition in a Separated Laminar Boundary Layer," *Journal of Fluid Mechanics*, Vol. 25, No. 4, 1966, pp. 683–704. doi:10.1017/S002211206600034X
[67] Braza, M., Faghani, D., and Persillon, H., "Successive Stages and the Role of Natural Vortex Dislocations in Three-Dimensional Wake Transition," *Journal of Fluid Mechanics*, Vol. 439, July 2001, pp. 1–41. doi:10.1017/S002211200100458X

P. G. Tucker
Associate Editor